Geophysical Research Letters

RESEARCH LETTER
10.1029/2024GL108267

Exploring the Behaviors of Initiated Progressive Failure and Slow-Moving Landslides in Los Angeles Using Satellite InSAR and Pixel Offset Tracking

Xiang Li[1], **Alexander L. Handwerger**[1,2], **Gilles Peltzer**[2,3], **and Eric Fielding**[2]

[1]Joint Institute for Regional Earth System Science and Engineering, University of California, Los Angeles, CA, USA, [2]Jet Propulsion Laboratory, California Institute of Technology, Pasadena, CA, USA, [3]Earth, Planetary and Space Sciences, University of California Los Angeles, Los Angeles, CA, USA

Key Points:

- We used satellite remote sensing to characterize the precursory motion of a catastrophic landslide
- Progressive failures and slow-moving landslides can be distinguished by analyzing their time-dependent motion
- Special attention should be given to landslides where no apparent historical movement has occurred

Supporting Information:

Supporting Information may be found in the online version of this article.

Correspondence to:

X. Li,
xiangli23@g.ucla.edu

Citation:

Li, X., Handwerger, A. L., Peltzer, G., & Fielding, E. (2024). Exploring the behaviors of initiated progressive failure and slow-moving landslides in Los Angeles using satellite InSAR and pixel offset tracking. *Geophysical Research Letters*, *51*, e2024GL108267. https://doi.org/10.1029/2024GL108267

Received 10 JAN 2024
Accepted 31 MAY 2024
Corrected 8 AUG 2024

This article was corrected on 8 AUG 2024. See the end of the full text for details.

Abstract Catastrophic landslides are often preceded by slow, progressive, accelerating deformation that differs from the persistent motion of slow-moving landslides. Here, we investigate the motion of a landslide that damaged 12 homes in Rolling Hills Estates (RHE), Los Angeles, California on 8 July 2023, using satellite-based synthetic aperture radar interferometry (InSAR) and pixel tracking of satellite-based optical images. To better understand the precursory motion of the RHE landslide, we compared its behavior with local precipitation and with several slow-moving landslides nearby. Unlike the slow-moving landslides, we found that RHE was a first-time progressive failure that failed after one of the wettest years on record. We then applied a progressive failure model to interpret the failure mechanisms and further predict the failure time from the pre-failure movement of RHE. Our work highlights the importance of monitoring incipient slow motion of landslides, particularly where no discernible historical displacement has been observed.

Plain Language Summary Landslides exhibit a wide range of behaviors around the world. Some landslides travel slowly downslope (velocities <1 m/yr) over a period of years or even decades. In contrast, other landslides fail catastrophically and travel downslope at high rates (>1 m/s), claiming lives and causing major damages. In some cases, these catastrophic landslides also display a precursory period of slow movement which presents an opportunity to detect them before they rapidly collapse. Here we investigated the movement of the Rolling Hills Estates (RHE) landslide, Los Angeles, California, before it moved many meters and damaged more than 12 houses on 8 July 2023. This landslide occurred after one of the wettest years on record in California. We found that the RHE landslide started sliding in 2023 in response to relatively high precipitation without obvious signs of movement in the three years preceding this event. This behavior differed starkly from the persistent motion of nearby slow-moving landslides that experienced nearly identical rainfall conditions. Our findings show that the RHE can be defined as a progressive failure and its failure time can be estimated approximately through analyzing its movement before the occurrence of the failure.

1. Introduction

Various types of landslides occur worldwide, each characterized by distinct pre-, syn-, and post-failure behaviors (Hungr et al., 2014). Some landslides display continuous movement at low velocities, typically less than 1 m/yr, exhibiting modest velocity variations driven by local climate conditions (Cascini et al., 2010; Handwerger et al., 2013; Hilley et al., 2004). On the other hand, some landslides experience rapid acceleration and catastrophic failure, reaching velocities even higher than a few m/s (Hendron & Patton, 1985; Schuster et al., 2002; Stark et al., 2017). It has been observed that these catastrophic landslide events are sometimes preceded by slow creeping movements (Lacroix et al., 2023; Stark et al., 2017; Voight, 1978). Therefore, it is important to examine which types of slope movement can develop into catastrophic failure and to further explore the associated triggering conditions. With this motivation, we analyzed the time-dependent motion of a landslide that occurred in Rolling Hills Estates (RHE) (KCAl-News staff, 2023), on the Palos Verdes Peninsula, Los Angeles, California, USA on 8 July 2023. The landslide destroyed 12 homes, valued between $1.1 and $1.4 million each. The 2023 water year, defined as the period from 1 October 2022, to 30 September 2023, was an extremely wet year that followed two of the driest water years on record (California Department of Water Resources, 2023). This sharp change from dry-to-wet is known as a "whiplash" and is predicted to become more common in California due to ongoing climate change (Swain et al., 2018). The first report of damage associated with RHE landslide were from

reports of cracks in an impacted house in April 2023 (Jacobs, 2023), indicating pre-failure creeping movement at this site. These findings establish RHE as a promising case for investigating pre-failure landslide motion.

While the RHE landslide was a notable event, the Palos Verdes Peninsula is known for landslides. Located just 3 km away, the slow-moving Portuguese Bend landslide (PBL) has been moving for more than 60 years (Merriam, 1960) and has been the topic of several previous investigations (e.g., Bouali et al., 2019; Calabro et al., 2010; Kayen et al., 2002; Linden, 1989). There have been many other landslides on Palos Verdes, and on 3 October 2023, the city of Rancho Palos Verdes declared a local emergency due to the landslides (Castleman, 2023). In addition, landslides are a major issue throughout all the California Coast Ranges (e.g., Handwerger et al., 2022). There are hundreds to thousands of active slow-moving landslides in California that result from high seasonal rainfall, weak rocks, and active tectonics (Keefer & Johnson, 1983; Roering et al., 2015; Scheingross et al., 2013). Thus, California provides an ideal location to examine differences between slow- and fast-moving landslides.

To better understand slow- and fast-motion exhibited by landslides, we perform detailed investigation of six active landslides in the Los Angeles area between 2016 and 2023. All of these landslides occur in a relatively dry region of California (mean annual rainfall ~ 300 mm/yr) that receives seasonal rainfall, primarily between November and April. We compare the record of landslide motion with local rainfall conditions to understand how year-to-year changes in seasonal rainfall impact landslide behaviors. We then examine differences in behavior between RHE and the five slow-moving landslides and test the commonly used inverse velocity method (Fukuzono, 1985; Lacroix et al., 2023) to determine if the rapid motion RHE could have been predicted in advance.

2. Methods

2.1. InSAR Processing

We identified and monitored landslide motion using InSAR time series between January 2016 and July 2023. We used SAR data acquired by the C-band (5.6 m radar wavelength) Copernicus Sentinel-1 (S1) A/B satellites. The S1 A/B constellation had a minimum repeat acquisition interval of 6 days between 2016 and 2021, when both S1 A/B were active. Note that S1B became unresponsive in late December 2021, which increased the minimum repeat acquisition time to 12 days. We processed data on both ascending (satellites moving north looking east) and descending (satellites moving south looking west) tracks. The data were processed using the InSAR Scientific Computing Environment (ISCE) version 2 software package developed at Jet Propulsion Laboratory (JPL)/Caltech (Rosen et al., 2012). We used the 30 m digital elevation model (DEM) from the Copernicus Global DEM (https://registry.opendata.aws/copernicus-dem/) to remove topographic contributions to the phase and to geocode the interferograms. We processed the data with two looks (~31 m pixel) in azimuth and seven looks in range (~16 m pixel) (Figure 1). Due to its small size (discussed in Section 3), we then reprocessed data at higher spatial resolution for RHE using one look in azimuth (~16 m pixel) and five looks in range (~12 m pixel). Finally, we performed an InSAR time series inversion using the Miami InSAR Time-series software in Python (MintPy) (Yunjun et al., 2019) with the small-baseline subset (SBAS) method. MintPy applies standard corrections to the InSAR time series including troposphere correction (Doin et al., 2009; Jolivet et al., 2011, 2014) and topographic residual correction (Fattahi & Amelung, 2013). For each landslide we selected a local stable reference point within 500 m of the active landslide body.

2.2. Pixel Offset Tracking

We also performed pixel offset tracking time series using 3 m PlanetScope optical images for RHE for only a few days before and after its catastrophic acceleration. The goal of this analysis was to measure the larger motions associated with its rapid acceleration. We selected six cloud free images between July 4 and 14, 2023 to track the pre- and post-failure motion of the landslide. PlanetScope images are orthorectified and have undergone radiometric, geometric, and sensor corrections (Planet Team, 2017). To measure offsets between images, we performed image correlation on 15 pairs of images, with time intervals ranging from 1 to 10 days (Table S2). We calculated pixel offsets using the Outlier-Resistant Correlator (OR-Corr) subpixel image correlation method developed by Milliner and Donnellan (2020). We used a 33 by 33-pixel correlation window with a step size of 9 pixels, resulting in displacement maps with a resolution of 27 m per pixel. Finally, we used the MintPy time series software to invert time-dependent motion of the landslide.

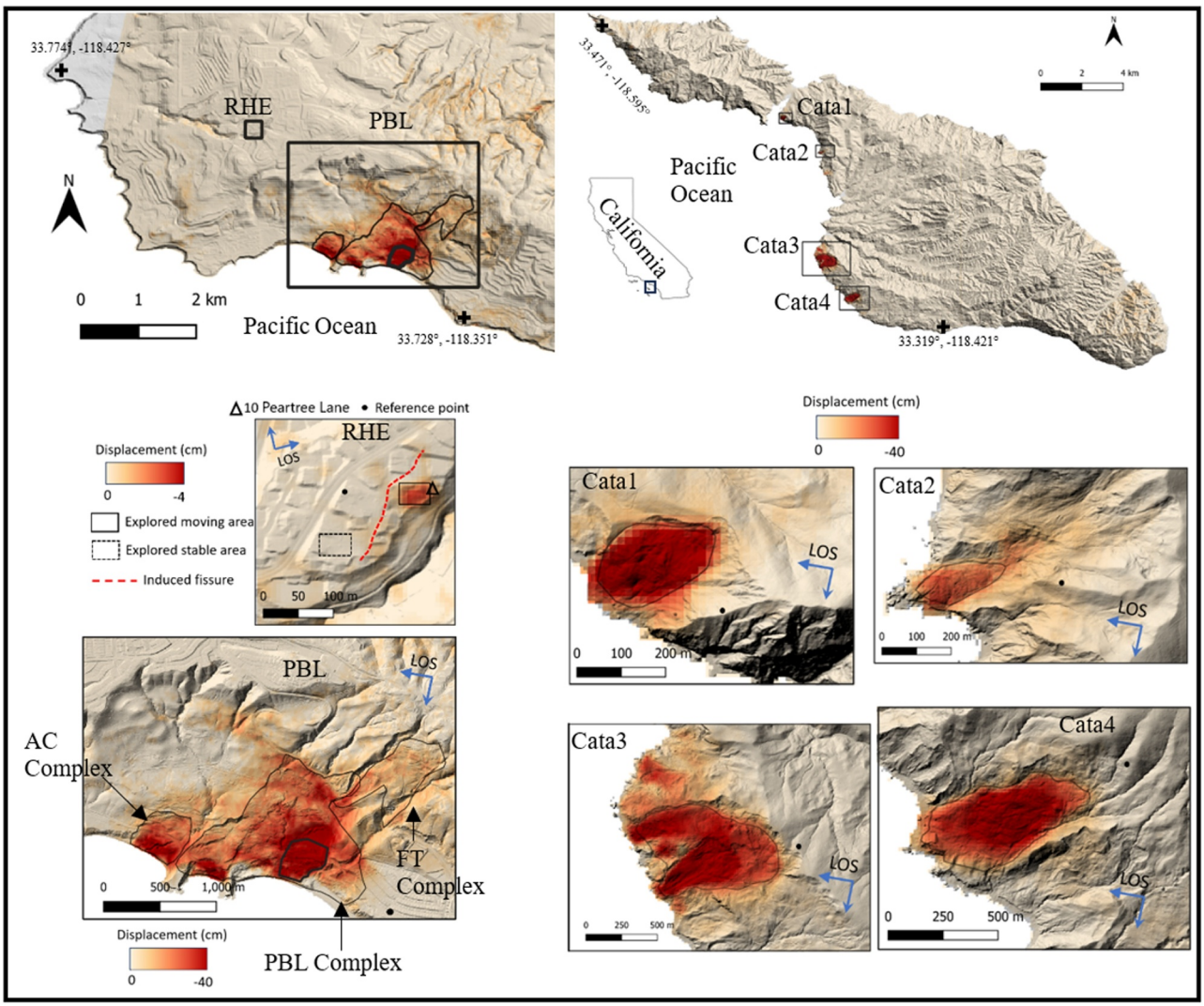

Figure 1. Displacement map for the Los Angeles area landslides. Insets show the zoomed in displacement map of Rolling Hills Estates landslide (ascending, 2022 July to 2023 June 25). The other insets show the displacement map of Portuguese Bend landslide landslide and the four identified landslides on Santa Catalina Island (from 2016 to2023 June 25). Black dots indicate the reference point for each map. Displacement maps are draped on lidar hillshades. More information about each case is in Table S1 in Supporting Information S1.

3. Results

3.1. Landslide Activity in the Los Angeles Region

We identified six active landslides in southern Los Angeles County between Palos Verdes Peninsula and Catalina Island (Figure 1). The four landslides on Catalina Island have not been previously inventoried (to our best knowledge). The westward downslope movement of PBL and the Catalina Island landslides was best imaged by the west-looking descending satellite pass, while the eastward downslope motion of RHE before the failure occurrence was best imaged by the east-looking ascending satellite pass. The RHE pre-failure mobilized area is relatively small, with an area of around 1,400 m^2 (average slope angle 13°), while the other five landslides are much larger features consisting of landslide complexes with multiple active zones ranging in area from 2.4×10^4 m^2 to 1.4×10^6 m^2 (with average slope angle from 16 to 23°, Table S1 in Supporting Information S1). Both of the landslides on Palos Verdes (RHE and PBL) occur within Miocene shales (Ehlig et al., 1992), and the landslides on Catalina Island occur within the Franciscan Mélange (maps.conservation.co.gov/cgs), a clay-rich complex unit known for causing slow-moving landslides (Handwerger et al., 2022; Kelsey, 1978).

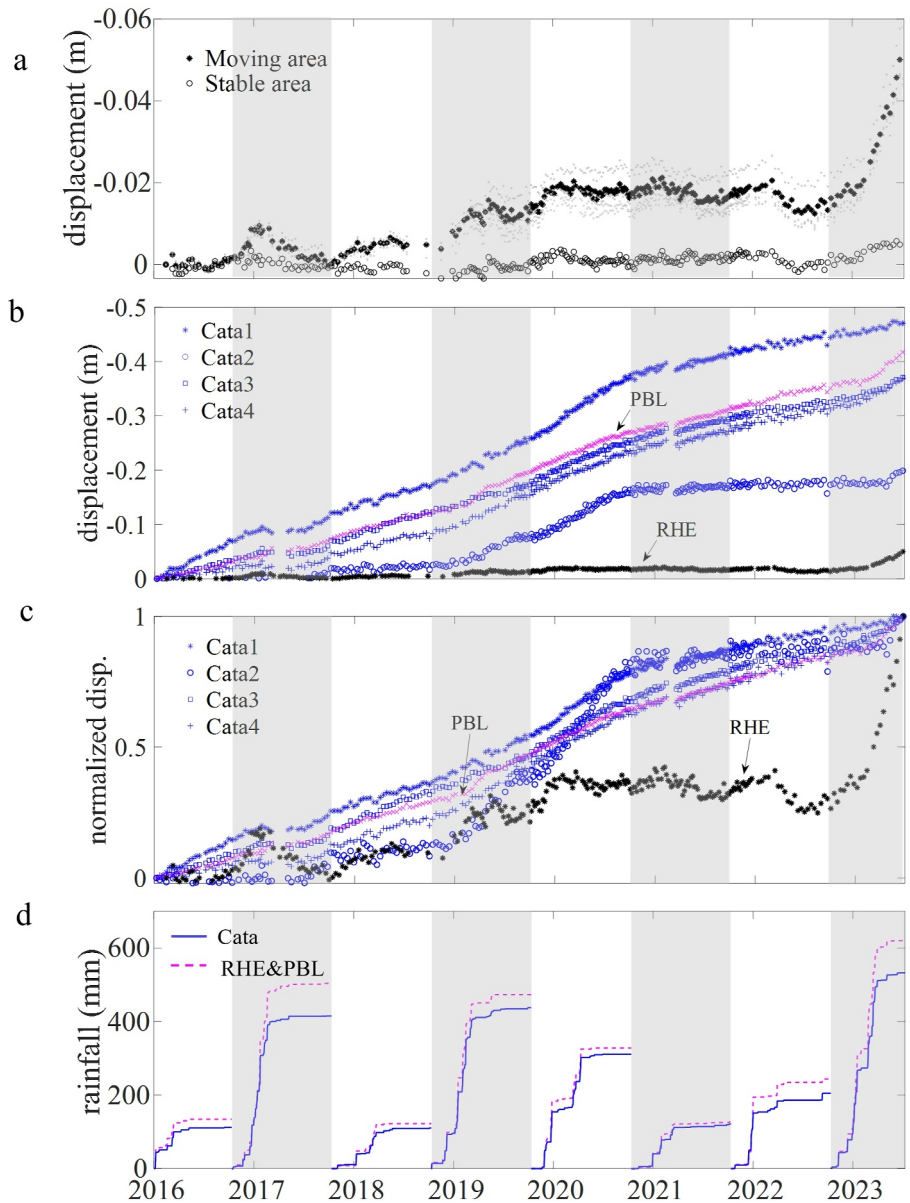

Figure 2. Displacement and precipitation time series. (a) Average LOS displacement time series for moving (black asterisk) and stable areas (gray open circles) of Rolling Hills Estates landslide, the displacement for the six moving pixels are also shown by light gray dots. (b) Displacement time series of Portuguese Bend landslide and the four landslides on Catalina Island. (c) Normalized displacement (divided by each maximum) of all studied cases. (d) Cumulative rainfall of each water year for Catalina and Palos Verdes from PRISM.

3.1.1. The Rolling Hills Estates Landslide

The InSAR times series at RHE reveals clear motion with around 0.04 m total displacement in the radar line-of-sight (LOS) direction from February 13 to 25 June 2023 (Figure 1). The moving area detected by our InSAR analysis is co-located with the area of cracks observed by local residents since April at 10 Peartree Lane (Jacobs, 2023). We also observed more subtle motion (<2 cm) during the 2019 wet season, however there are no reports we could find to confirm these findings. Notably, the displacement time series of RHE does exhibit some fluctuations (magnitude <1 cm) between 2016, 2017, and 2019 (Figure 2). However, similar fluctuations are observed when looking at the time series of a stable area nearby the landslide (Figure 2a). Thus, we attribute these fluctuations to error in the time series likely resulting from soil moisture changes (De Zan et al., 2015).

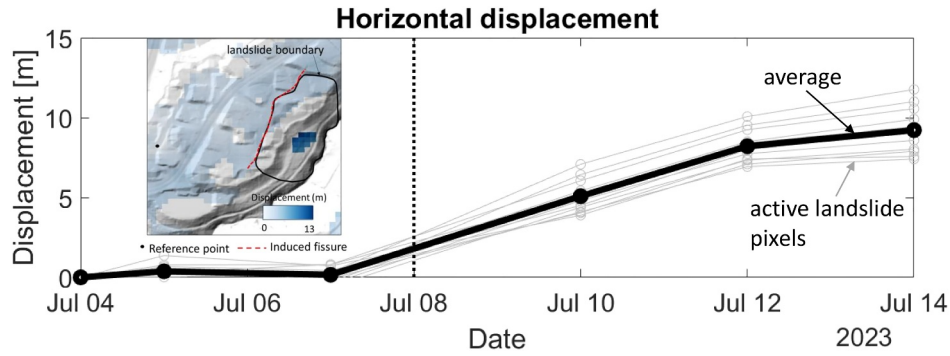

Figure 3. Displacement time series of the fastest moving area obtained from pixel tracking, the inset shows the displacement map from July 4 to 14 July 2023. The vertical dashed line corresponds to the major failure that occurred on 8 July 2023.

Comparing the displacement time series to the local precipitation from Parameter-elevation Regression on Independent Slopes Model (PRISM) (Figure 2) shows RHE is hydraulically driven. The landslide first moved slightly in the wet season of 2019 and then initiated its motion toward failure during the unusually wet season of 2023. There is a delay between the onset of precipitation and the onset of ground movement in both cases. Most rainfall in the 2023 water year fell between December 2022 and March 2023, yet the obvious ground movement initiated around February 2023 (~2-month lag from the rainfall start). The RHE failure also occurred on a dry sunny day (July 8) that followed a 40-day period of no significant rainfall. A delayed response has also been observed at many other landslides observed in California (e.g., Handwerger et al., 2013; Hilley et al., 2004; Iverson & Major, 1987).

In addition to the InSAR analysis, we examined the displacement time series from pixel offset tracking of 3 m PlanetScope imagery (Figure 3). The pixel tracking results reveal little to no motion between July 4 and July 7, which is likely because any motion that occurred was less than the detectable limit of the method (1/10 pixel size = 30 cm). This observation agrees with 4 cm LOS displacements measured by InSAR. However, the pixel tracking data are able to capture the post-failure motion between July 7 and July 14 where up to ~12 m of horizontal motion occurred, leading to the destruction of 12 homes.

3.1.2. Time-Dependent Motion of the Los Angeles Region Landslides

To better understand the time-dependent behavior of the RHE landslide, we compared RHE to the five nearby slow-moving landslides. These landslides all experienced similar rainfall conditions (Figure 2d). Average annual rainfall at these sites is around 0.3 m in the PRISM database. Each of the landslides exhibited seasonal changes in velocity driven by changes in rainfall between 2016 and 2023. The landslides were also sensitive to year-to-year changes in rainfall, most of them exhibit the largest displacements in the wetter years 2017, 2019, 2020, and 2023. We also observed some differences in behavior between the five slow-moving landslides. We found the CATA1 landslide did not respond to the 2023 rainfall and that the CATA2 landslide showed more episodic motion compared to the others with more than 90% of its total motion occurring in the four wetter years. The other four slow-moving landslides exhibited more continuous displacement with less pronounced year-to-year changes. Reasons that can lead to these distinct behaviors under similar precipitation conditions are analyzed in Section 5 below. While much of this was known about the PBL complex (e.g., Calabro et al., 2010; Merriam, 1960), this is the first documentation of the active slow-moving landslide behaviors on Catalina Island.

We also explored relative differences in motion between the landslides by examining the normalized displacement time series (Figure 2c). Looking at relative changes in motion, we found that only RHE experienced considerably higher displacement (more than 60% of the total displacement in seven years) in 2023. For the other cases, the movement during 2023 takes only around 5%–20% of each total displacement. Comparing all six landslides shows conclusively that RHE's behavior was different in that it was characterized by a pronounced movement in 2023 with little to no prior motion during the study period. These findings suggest that RHE can be classified as a progressive failure.

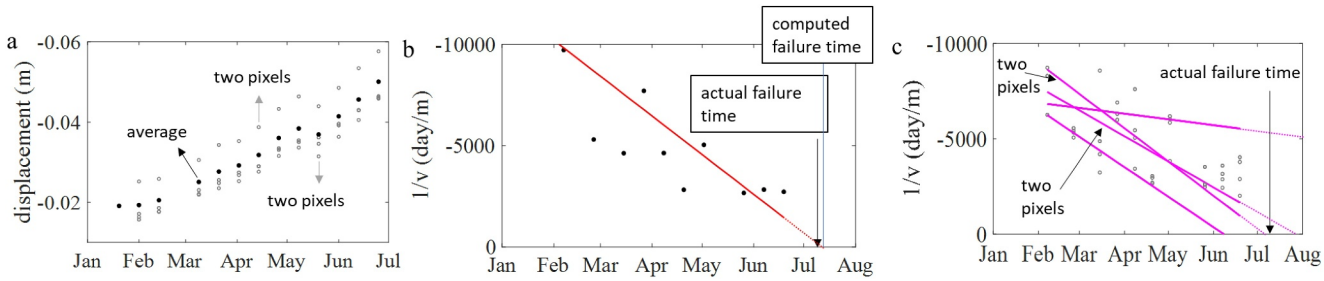

Figure 4. Inverse velocity analyses. (a) Rolling Hills Estates displacement time series measurement after January 2023. (b) weighted linear regression on the inverse velocity (only display from 0 to -1×10^4) computed from the average displacement against time. (c) weighted linear regression on the inverse velocity computed from each of the pixels showing precursory movement.

4. Progressive Failure Investigation

Landslide forecasting, especially the temporal prediction of failure is a major challenge (Bell, 2018; Intrieri et al., 2019). Empirical and semi-empirical methods have been used to forecast ground failure time based on its pre-failure velocity and/or acceleration (e.g., Fukuzono, 1985; Lei et al., 2023; Saito, 1969; Voight, 1989). In particular, the inverse velocity method has been widely applied, which shows that in certain cases the inverse velocity decreases linearly toward zero and can be used to forecast ground failure time (Intrieri et al., 2019; Lacroix et al., 2023). Petley et al. (2005) analyzed experiments on a clayey slope to investigate the relationship between velocity and the growth of a landslide shear surface. The experiment revealed that the shear surface growth initiated when the pore-water pressure exceeded a threshold and stopped growing if the pore-water pressure dropped beneath the threshold value. Failure of the slope eventually occurred once the shear surface was fully developed when the pore-water pressure was relatively high. Importantly, Petley et al. (2005) showed how progressive failures develop due to stress perturbations and that the inverse velocity method can be used to forecast this type of progressive failure.

Next, we examine the RHE landslide in the context of a progressive failure to see if failure time could have been forecast based on only its pre-failure movement. For this analysis, we focus on the landslide motion from February 2023 forwards, when obvious displacement started to develop. We perform this analysis using the following steps: (a) we calculate velocity time series from the average and individual displacement of the six pixels exhibiting obvious precursory movement (Figure 4a) using a central difference method. We chose this method because of its accuracy and efficiency in computing derivatives. (b) As previously mentioned, the displacement observation might be biased by soil moisture changes or other sources of noise in the data (e.g., Yunjun et al., 2019). Here, in order to reduce the impact of noise, we conduct weighted linear regression on the inverse velocity against time with sample weights computed from inverse-variance (Figure 4b). (c) As Petley et al. (2005) implemented, progressive failure time can be obtained when the linear trend of 1/v approaches zero. In this context, such a time can be computed from the linear regression coefficients in step 2 by dividing the absolute value of the intercept by the gradient. The predicted failure time using the average displacement is July 11, 3 days later than the actual failure time (Figure 4b). However, due to the data noise and low number of samples, adding or subtracting one standard deviation on the average displacement will lead to two greatly different failure times, June 14 and November 28, respectively. In this context, to better analyze the precursory movement, the failure time from each pixel is also computed. As illustrated in Figure 4c, the computed failure times are June 7, July 4, July 4, July 25, July 25, and January 8 (2025), with a median failure time on July 14, 6 days after the actual failure. Our analysis indicates that the approximate failure time of RHE can be back computed based on its pre-failure movement. However, there is significant uncertainty in this prediction due to a low signal-to-noise ratio in the InSAR data and limited number of pixels available for analysis. While our results are encouraging, predicting the failure time from satellite remote sensing data needs more validation worldwide (e.g., Intrieri et al., 2019; Lacroix et al., 2023). Nonetheless, we emphasize that for ground deformation sites where no historical movement has occurred, progressive failure is a significant concern that requires close attention.

5. Discussion

Satellite InSAR is an ideal tool for measuring the velocities and velocity changes of slow-moving landslides and identifying progressive failures such as RHE. For slow-moving landslides that persist for months or longer, satellite InSAR can be used to track their motion and better understand landslide processes in general. For progressive failures, satellite InSAR can be used to warn of catastrophic failure if the landslide develops over a period of weeks to months (i.e., multiple satellite overpasses). However, not all landslides exhibit precursory motion over this time period and would require other tools, such as ground based instruments, to detect them before failure (Bell, 2018; Intrieri et al., 2019).

The temporal prediction of landslide failure time is both significant and challenging. RHE failed catastrophically, while five nearby slow-moving landslides continue to slide slowly. There are several factors that can lead to the stable creeping movement such as: dilation-induced negative pore-water pressure (Iverson, 2005; Li et al., 2023), thermo-dynamic coupling (Veveakis et al., 2007), and rate-strengthening friction (Alonso et al., 2016; Handwerger et al., 2016). Whether a landslide will move slowly or fail catastrophically is not controlled by its size. Therefore, although the pre-failure active zone of RHE is relatively small, it has no direct influence on the final collapse. From our remote sensing data alone, we cannot determine the mechanisms that control these disparate behaviors. Despite these limitations, it appears clear that high rainfall during the unusually wet 2023 water year played a major factor in the RHE behavior. We also note that the RHE landslide occurred in a suburban area with significant infrastructure that can alter natural drainage paths (Dille et al., 2022). We cannot determine if human impact played a role in the RHE landslide from our remote sensing data set. A detailed investigation of ground-based data is needed to make such a determination.

We identified the RHE landslide as a first-time progressively failing landslide. In agreement with the progressive failure model put forth by Petley et al. (2005), we hypothesize that RHE exhibited a small amount of movement when the shear surface was in development. Once the shear surface formed, the landslide transitioned to global movement which ultimately led to the destruction of 12 homes and millions of dollars in damages. This is distinct from the slow-moving landslides, which can move persistently even in years with less rainfall. Notably, the movement of CATA2 exhibited more episodic, albeit slow, motion. CATA2 moved significantly in 2019 for the first time in our study period. This behavior may have been initially interpreted as a progressive failure if we were monitoring the site in real time. However, analysis of the time-dependent motion shows the landslide did not exhibit the runaway acceleration pattern typical of progressive failures.

We observed behavioral differences between the five slow-moving landslides. These slow-moving landslides displayed variation in the timing and magnitude of motion during each rainy season even though they all occurred under similar environmental conditions. We attribute these kinematic behaviors to different landslide properties such as geometry (Handwerger et al., 2021), hydraulic diffusivity (Iverson & Major, 1987), and mechanical properties such as strength and dilatancy (Iverson, 2005; Li et al., 2023). Previous work has shown that the hydraulic permeability (directly related to hydraulic diffusivity) at the same landslide site can vary by five orders of magnitude (Iverson & Major, 1987). It is thus not surprising that landslide materials in different sites can possess distinct diffusivity, which can lead to various pore-water pressure trends.

Lastly, our work on the Los Angeles region landslides shows that precipitation swings have a major impact on slow- and fast-moving landslides. Our findings also indicate that rainfall from previous seasons controls landslide behavior (e.g., 2019–2020 water year). These findings agree with recent work on landslides in other parts of California (e.g., Handwerger et al., 2022) and around the world (Cascini et al., 2010; Conte et al., 2017), and further show that climate change will alter landslide occurrence and behavior. Climate change models for California predict that precipitation patterns are evolving toward periods of extreme drought and extreme rainfall (Swain, 2021; Swain et al., 2018). The transition from dry to wet seasons can alter landslide behaviors and may exacerbate the triggering of catastrophic landslides. The extended dry season can open cracks to make water penetrate deeper, leading to stronger pore pressure changes in the wet season. It can also accelerate the weathering of earthen material. In this context, using satellite imagery to obtain high resolution ground deformation measurements presents abundant opportunities to explore the hydro-mechanical models governing earthen material behaviors, thereby improving the geo-hazard early warning systems in the face of climate extremes.

6. Conclusion

We studied six landslides in the Los Angeles Area, with a focus on the RHE landslide that destroyed 12 homes in Rancho Palos Verdes. We examined other slow-moving landslides nearby that occur under similar environmental conditions to better understand how slow movement can transition into catastrophic failure. Most of these slow-moving landslides moved at a rate of a few cm/yr and exhibited larger deformation rates in wetter years.

By analyzing the movement time history of RHE, we found that RHE is a progressive failure event. We propose that the behavior exhibited by RHE can be explained by the growth of the shear surface. We estimated the time of failure by analyzing the observed movement. Although the reliability of using InSAR to predict failure time needs more cases to validate worldwide, our results show that the timing of catastrophic failure of RHE could have been estimated within a few days of actual failure. Our findings provide further evidence that satellite remote sensing data can contribute to landslide early warning systems and can also be used to better understand the impacts of climate change on landslide hazards.

Data Availability Statement

Sentinel-1 data are available at https://search.asf.alaska.edu/#/, the ASF data search vertex. The InSAR Scientific Computing Environment (ISCE) software is available at https://github.com/isce-framework/isce2. The optical images used for pixel offset tracking were downloaded from PlanetScope optical images using an Education and Research Program license, at https://developers.planet.com/docs/data/planetscope/. The full list of interferograms used to generate movement time series are shown in Table S2. The landslide inventory metrics are included in Table S1 in Supporting Information S1. Precipitation data is provided by Parameter-elevation Regression on Independent Slopes Model (PRISM) available at https://prism.oregonstate.edu/. The Miami INsar Time-series software in Python (MintPy) is available at https://github.com/insarlab/MintPy. DEM shown in Figure 1 were USGS Lidar DEM, downloaded from OpenTopography at https://portal.opentopography.org/datasets.

Acknowledgments

We thank Sophia Winter for working on the identification of the landslides on Catalina Island during an undergraduate research project at UCLA. We also thank two anonymous reviewers and the editor for constructive reviews that improved the manuscript. PlanetScope images were provided by Planet's Education and Research Program to ALH. This work contains modified Copernicus Sentinel data 2016–2023, processed by ESA. Part of this research was supported by NSF PREEVENTS Grant 2023112. Part of this research was carried out at the Jet Propulsion Laboratory, California Institute of Technology, under a contract with the National Aeronautics and Space Administration (80NM0018D0004), and supported by the Earth Surface and Interior program.

References

Alonso, E., Zervos, A., & Pinyol, N. (2016). Thermo-poro-mechanical analysis of landslides: From creeping behaviour to catastrophic failure. *Géotechnique*, *66*(3), 202–219. https://doi.org/10.1680/jgeot.15.lm.006

Bell, A. F. (2018). Predictability of landslide timing from quasi-periodic precursory earthquakes. *Geophysical Research Letters*, *45*(4), 1860–1869. https://doi.org/10.1002/2017gl076730

Bouali, E. H., Oommen, T., & Escobar-Wolf, R. (2019). Evidence of instability in previously-mapped landslides as measured using GPS, optical, and SAR data between 2007 and 2017: A case study in the Portuguese bend landslide complex, California. *Remote Sensing*, *11*(8), 937. https://doi.org/10.3390/rs11080937

Calabro, M., Schmidt, D., & Roering, J. (2010). An examination of seasonal deformation at the Portuguese Bend landslide, Southern California, using radar interferometry. *Journal of Geophysical Research*, *115*(F2). https://doi.org/10.1029/2009jf001314

California Department of Water Resources. (2023). *Water Year 2023: Weather whiplash, from drought to Deluge*. California Natural Resources Agency.

Cascini, L., Calvello, M., & Grimaldi, G. M. (2010). Groundwater modeling for the analysis of active slow-moving landslides. *Journal of Geotechnical and Geoenvironmental Engineering*, *136*(9), 1220–1230. https://doi.org/10.1061/(asce)gt.1943-5606.0000323

Castleman, T. (2023). *Rancho Palos Verdes declares emergency after landslides; more damage feared in upcoming winter* (Vol. 6). Los Angeles Times. Retrieved from https://www.latimes.com/california/story/2023-10-06/rancho-palos-verdes-declares-emergency-following-landslides-worries-about-more-damage-during-upcoming-winter?_gl=1*t6vyla*_gcl_au*MTM4MjAwMDA4Ny4xNjk2NDU1MzMy

Conte, E., Donato, A., & Troncone, A. (2017). A simplified method for predicting rainfall-induced mobility of active landslides. *Landslides*, *14*(1), 35–45. https://doi.org/10.1007/s10346-016-0692-8

De Zan, F., Zonno, M., & Lopez-Dekker, P. (2015). Phase inconsistencies and multiple scattering in SAR interferometry. *IEEE Transactions on Geoscience and Remote Sensing*, *53*(12), 6608–6616. https://doi.org/10.1109/tgrs.2015.2444431

Dille, A., Dewitte, O., Handwerger, A. L., d'Oreye, N., Derauw, D., Ganza Bamulezi, G., et al. (2022). Acceleration of a large deep-seated tropical landslide due to urbanization feedbacks. *Nature Geoscience*, *15*(12), 1048–1055. https://doi.org/10.1038/s41561-022-01073-3

Doin, M.-P., Lasserre, C., Peltzer, G., Cavalié, O., & Doubre, C. (2009). Corrections of stratified tropospheric delays in SAR interferometry: Validation with global atmospheric models. *Journal of Applied Geophysics*, *69*(1), 35–50. https://doi.org/10.1016/j.jappgeo.2009.03.010

Ehlig, P., Pipkin, B., & Proctor, R. (1992). Evolution, mechanics and mitigation of the Portuguese Bend landslide. In *Palos Verdes Peninsula, California. Engineering geology practice in Southern California* (pp. 531–553). Star Publishing Co.

Fattahi, H., & Amelung, F. (2013). DEM error correction in InSAR time series. *IEEE Transactions on Geoscience and Remote Sensing*, *51*(7), 4249–4259. https://doi.org/10.1109/tgrs.2012.2227761

Fukuzono, T. (1985). A method to predict the time of slope failure caused by rainfall using the inverse number of velocity of surface displacement. *Landslides*, *22*(2), 8–13_11. https://doi.org/10.3313/jls1964.22.2_8

Handwerger, A. L., Booth, A. M., Huang, M. H., & Fielding, E. J. (2021). Inferring the subsurface geometry and strength of slow-moving landslides using 3-D velocity measurements from the NASA/JPL UAVSAR. *Journal of Geophysical Research: Earth Surface*, *126*(3), e2020JF005898. https://doi.org/10.1029/2020jf005898

Handwerger, A. L., Fielding, E. J., Sangha, S. S., & Bekaert, D. P. (2022). Landslide sensitivity and response to precipitation changes in wet and dry climates. *Geophysical Research Letters*, *49*(13), e2022GL099499. https://doi.org/10.1029/2022gl099499

Handwerger, A. L., Rempel, A. W., Skarbek, R. M., Roering, J. J., & Hilley, G. E. (2016). Rate-weakening friction characterizes both slow sliding and catastrophic failure of landslides. *Proceedings of the National Academy of Sciences*, *113*(37), 10281–10286. https://doi.org/10.1073/pnas.1607009113

Handwerger, A. L., Roering, J. J., & Schmidt, D. A. (2013). Controls on the seasonal deformation of slow-moving landslides. *Earth and Planetary Science Letters*, *377*, 239–247. https://doi.org/10.1016/j.epsl.2013.06.047

Hendron, A., Jr., & Patton, F. D. (1985). *The Vaiont slide. A geotechnical analysis based on new geologic observations of the failure surface*. US Army Corps of Engineers. (Vol. 1).

Hilley, G. E., Bürgmann, R., Ferretti, A., Novali, F., & Rocca, F. (2004). Dynamics of slow-moving landslides from permanent scatterer analysis. *Science*, *304*(5679), 1952–1955. https://doi.org/10.1126/science.1098821

Hungr, O., Leroueil, S., & Picarelli, L. (2014). The varnes classification of landslide types, an update. *Landslides*, *11*(2), 167–194. https://doi.org/10.1007/s10346-013-0436-y

Intrieri, E., Carlà, T., & Gigli, G. (2019). Forecasting the time of failure of landslides at slope-scale: A literature review. *Earth-Science Reviews*, *193*, 333–349. https://doi.org/10.1016/j.earscirev.2019.03.019

Iverson, R. M. (2005). Regulation of landslide motion by dilatancy and pore pressure feedback. *Journal of Geophysical Research*, *110*(F2). https://doi.org/10.1029/2004jf000268

Iverson, R. M., & Major, J. J. (1987). Rainfall, ground-water flow, and seasonal movement at minor creek landslide, Northwestern California: Physical interpretation of empirical relations. *The Geological Society of America Bulletin*, *99*(4), 579–594. https://doi.org/10.1130/0016-7606(1987)99<579:rgfasm>2.0.co;2

Jacobs, L. (2023). *Rolling Hills Estates landslide 'didn't just happen in an instant', says Peartree Lane resident*. Daily Breeze. Retrieved from https://www.dailybreeze.com/2023/07/14/rolling-hills-estates-landslide-didnt-just-happen-in-an-instant-says-peartree-lane-resident/

Jolivet, R., Agram, P. S., Lin, N. Y., Simons, M., Doin, M. P., Peltzer, G., & Li, Z. (2014). Improving InSAR geodesy using global atmospheric models. *Journal of Geophysical Research: Solid Earth*, *119*(3), 2324–2341. https://doi.org/10.1002/2013jb010588

Jolivet, R., Grandin, R., Lasserre, C., Doin, M. P., & Peltzer, G. (2011). Systematic InSAR tropospheric phase delay corrections from global meteorological reanalysis data. *Geophysical Research Letters*, *38*(17). https://doi.org/10.1029/2011gl048757

Kayen, R., Lee, H., & Hein, J. (2002). Influence of the Portuguese bend landslide on the character of the effluent-affected sediment deposit, Palos Verdes margin, Southern California. *Continental Shelf Research*, *22*(6–7), 911–922. https://doi.org/10.1016/s0278-4343(01)00111-x

Keefer, D. K., & Johnson, A. M. (1983). *Earth flows; morphology, mobilization, and movement* (Vol. 1264, pp. 2330–7102). US Geological Survey. https://doi.org/10.3133/pp1264

Kelsey, H. M. (1978). Earthflows in Franciscan melange, van Duzen River Basin, California. *Geology*, *6*(6), 361–364. https://doi.org/10.1130/0091-7613(1978)6<361:eifmvd>2.0.co;2

Lacroix, P., Huanca, J., Angel, L., & Taipe, E. (2023). Precursory motion and time-of-failure prediction of the achoma landslide, Peru, from high frequency PlanetScope satellites. *Geophysical Research Letters*, *50*(19), e2023GL105413. https://doi.org/10.1029/2023gl105413

Lei, Q., Sornette, D., Yang, H., & Loew, S. (2023). Real-time forecast of catastrophic landslides via dragon-king detection. *Geophysical Research Letters*, *50*(6), e2022GL100832. https://doi.org/10.1029/2022gl100832

Li, X., Chen, Y., Handwerger, A. L., & Buscarnera, G. (2023). Dynamics of creeping landslides controlled by inelastic hydro-mechanical couplings. *Engineering Geology*, *317*, 107078. https://doi.org/10.1016/j.enggeo.2023.107078

Linden, K. V. (1989). The Portuguese bend landslide. *Engineering Geology*, *27*(1–4), 301–373. https://doi.org/10.1016/0013-7952(89)90037-9

Merriam, R. (1960). Portuguese bend landslide, Palos Verdes Hills, California. *The Journal of Geology*, *68*(2), 140–153. https://doi.org/10.1086/626649

Milliner, C., & Donnellan, A. (2020). Using daily observations from Planet Labs satellite imagery to separate the surface deformation between the 4 July M w 6.4 foreshock and 5 July M w 7.1 mainshock during the 2019 Ridgecrest earthquake sequence. *Seismological Research Letters*, *91*(4), 1986–1997. https://doi.org/10.1785/0220190271

Petley, D. N., Higuchi, T., Petley, D. J., Bulmer, M. H., & Carey, J. (2005). Development of progressive landslide failure in cohesive materials. *Geology*, *33*(3), 201–204. https://doi.org/10.1130/g21147.1

Planet Team. (2017). *Planet application program interface: In Space for life on Earth*. Planet Team. Retrieved from https://api.planet.com

Roering, J. J., Mackey, B. H., Handwerger, A. L., Booth, A. M., Schmidt, D. A., Bennett, G. L., & Cerovski-Darriau, C. (2015). Beyond the angle of repose: A review and synthesis of landslide processes in response to rapid uplift, Eel river, Northern California. *Geomorphology*, *236*, 109–131. https://doi.org/10.1016/j.geomorph.2015.02.013

Rosen, P. A., Gurrola, E., Sacco, G. F., & Zebker, H. (2012). The InSAR scientific computing environment. In *EUSAR 2012; 9th European conference on synthetic aperture radar* (pp. 730–733). VDE.

Saito, M. (1969). Forecasting time of slope failure by tertiary creep. In *Paper presented at the proceedings of the 7th international conference on soil mechanics and foundation engineering*.

Scheingross, J. S., Minchew, B. M., Mackey, B. H., Simons, M., Lamb, M. P., & Hensley, S. (2013). Fault-zone controls on the spatial distribution of slow-moving landslides. *Bulletin*, *125*(3–4), 473–489. https://doi.org/10.1130/b30719.1

Schuster, R. L., Salcedo, D. A., & Valenzuela, L. (2002). Overview of catastrophic landslides of South America in the twentieth century. *Reviews in Engineering Geology*, *15*, 1–34. https://doi.org/10.1130/reg15-p1

KCAL-News staff. (2023). *Massive landslide destroys homes, prompts evacuations in Rolling Hills Estates neighborhood*. CBS. Retrieved from https://www.cbsnews.com/losangeles/news/massive-landslide-prompts-evacuations-in-rolling-hills-estates-neighborhood/

Stark, T. D., Baghdady, A. K., Hungr, O., & Aaron, J. (2017). Case study: Oso, Washington, landslide of March 22, 2014—Material properties and failure mechanism. *Journal of Geotechnical and Geoenvironmental Engineering*, *143*(5), 05017001. https://doi.org/10.1061/(asce)gt.1943-5606.0001615

Swain, D. L. (2021). A shorter, sharper rainy season amplifies California wildfire risk. *Geophysical Research Letters*, *48*(5), e2021GL092843. https://doi.org/10.1029/2021gl092843

Swain, D. L., Langenbrunner, B., Neelin, J. D., & Hall, A. (2018). Increasing precipitation volatility in twenty-first-century California. *Nature Climate Change*, *8*(5), 427–433. https://doi.org/10.1038/s41558-018-0140-y

Veveakis, E., Vardoulakis, I., & Di Toro, G. (2007). Thermoporomechanics of creeping landslides: The 1963 Vaiont slide, Northern Italy. *Journal of Geophysical Research*, *112*(F3). https://doi.org/10.1029/2006jf000702

Voight, B. (1978). *Rockslides and avalanches*. Elsevier Scientific Pub. Co.

Voight, B. (1989). A relation to describe rate-dependent material failure. *Science*, *243*(4888), 200–203. https://doi.org/10.1126/science.243.4888.200

Yunjun, Z., Fattahi, H., & Amelung, F. (2019). Small baseline InSAR time series analysis: Unwrapping error correction and noise reduction. *Computers and Geosciences*, *133*, 104331. https://doi.org/10.1016/j.cageo.2019.104331

10.1029/2024GL108267

Erratum

The originally published version of this article contained a typographical error. In the first sentence of the first paragraph of Section 3.1.1, "motion with around 0.4 m" should be changed to "motion with around 0.04 m." The error has been corrected, and this may be considered the authoritative version of record.